Supplementary Materials

Figure S1-S4. ^{1}H NMR spectrum of compound a, b, c, d, e, f, g and h. The tables D in each figure show the characteristic chemical shift both in reactants and products. “Existence” stood for the characteristic chemical shift co-contained by both reactants and products. “Disappearance” referred to the chemical bond only contained in the reactants, which disappeared in the reaction processes and did not exist in the products. “Formation” represented the chemical bonds only existing in the products, which newly generated in the chemical reaction processes and were not found in the reactants. Solvent peaks of NMR (Water 3.33ppm; Dimethyl sulfoxide 2.49 ppm; N, N-Dimethylformamide 7.95, 2.89, 2.73ppm; Deuterium solvent $(CD_3)_2SO$).

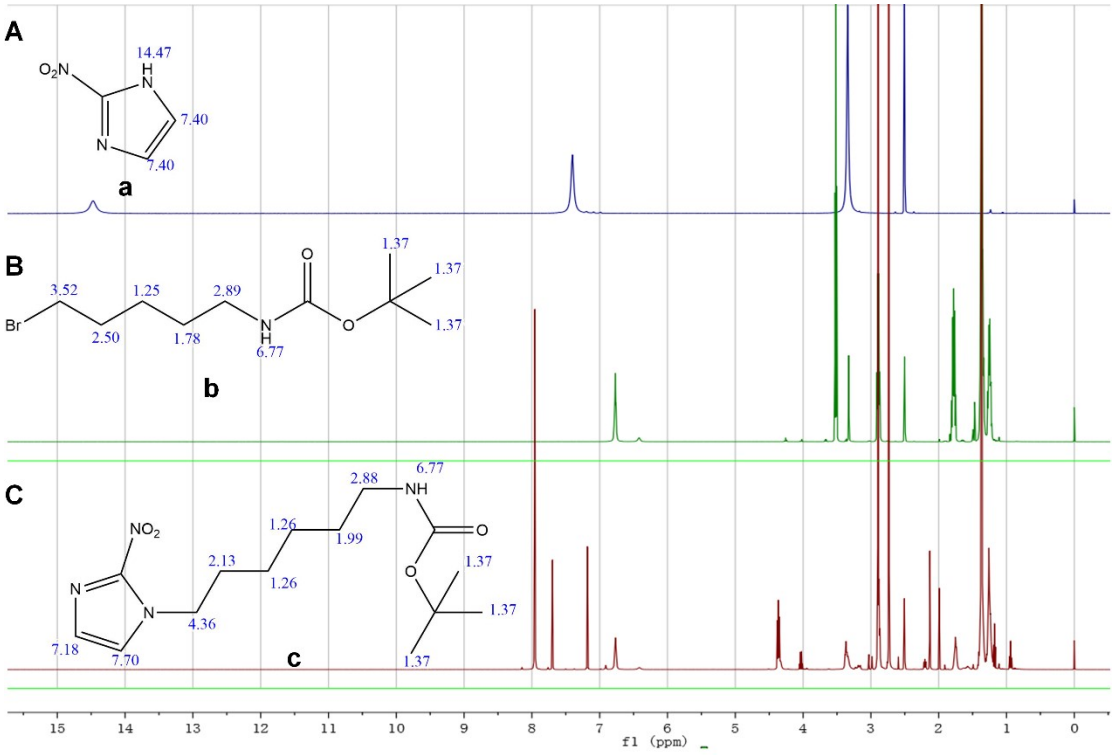

D

Compound	The characteristic chemical shift			
	Existence			Disappearance
a	-CH=CH- (7.40ppm)			-NH- (14.47ppm)
b		-O-CO-NH- (6.77ppm)	$-C(CH_3)_3$ (1.37ppm)	
c	-CH=CH- (7.18ppm , 7.70ppm)	-O-CO-NH- (6.77ppm)	$-C(CH_3)_3$ (1.37ppm)	

Figure S1

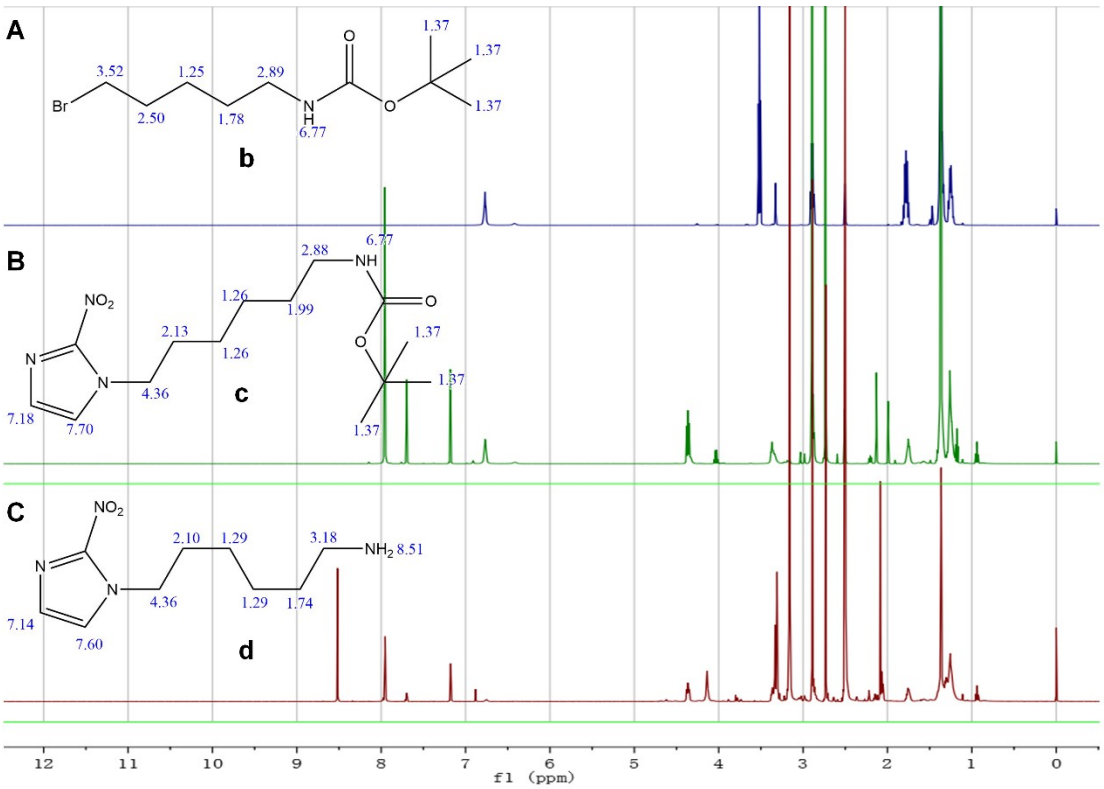

D

Compound	The characteristic chemical shift			
	Existence		Disappearance	Formation
c	-N-CH_2- (4.36ppm)	-CH=CH- (7.18ppm, 7.70ppm)	-O-CO-NH- (6.77ppm)	
d	-N-CH_2- (4.36ppm)	-CH=CH- (7.14ppm, 7.60ppm)		-NH_2 (8.51ppm)

Figure S2

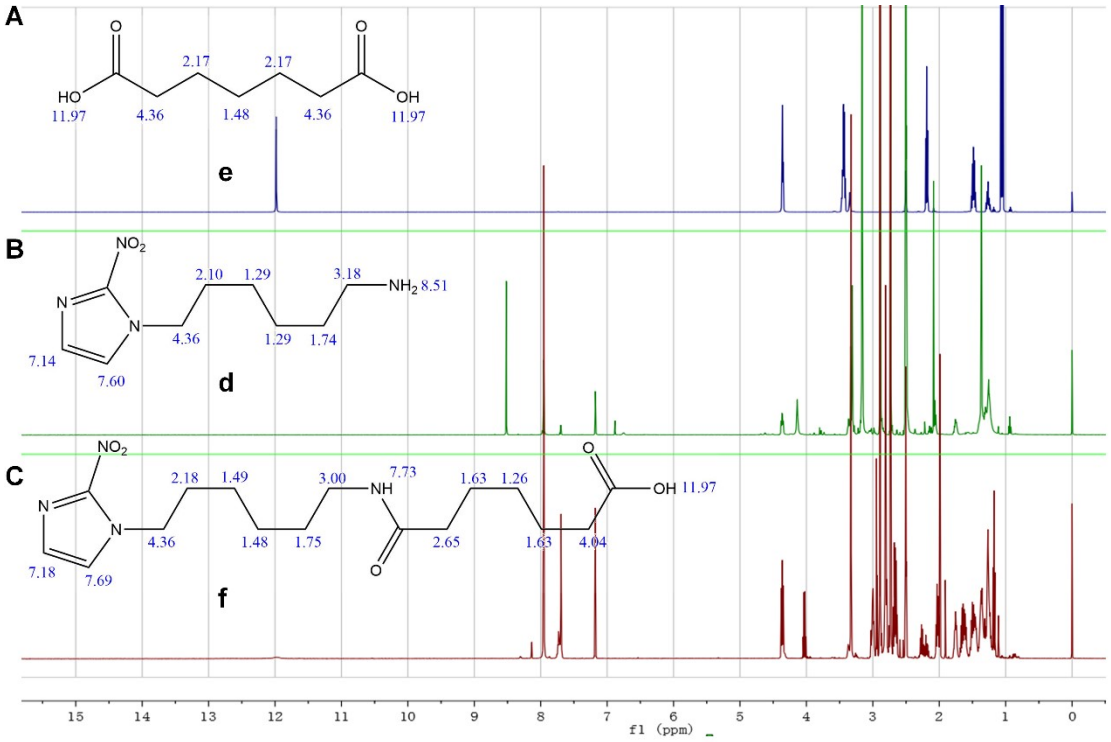

D

Compound	The characteristic chemical shift			
	Existence		Disappearance	Formation
d	-CH=CH- (7.14ppm, 7.60ppm)		$-NH_2$ (8.51ppm)	
e		-COOH (11.97ppm)		
f	-CH=CH- (7.18ppm, 7.69ppm)	-COOH (11.97ppm)		-NH-CO- (7.73ppm)

Figure S3

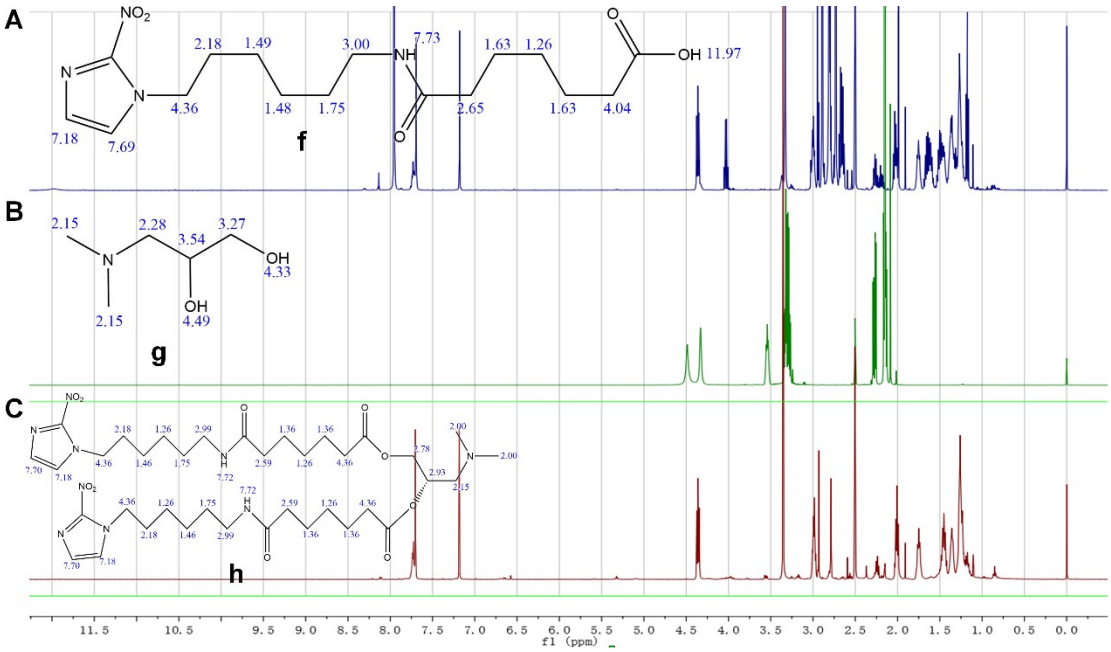

D

Compound	The characteristic chemical shift		
	Existence		Disappearance
f	-CH=CH- (7.18ppm, 7.69ppm)	-NH-CO- (7.73ppm)	-COOH (11.97ppm)
g			
h	-CH=CH- (7.18ppm, 7.70ppm)	-NH-CO- (7.72ppm)	

Figure S4

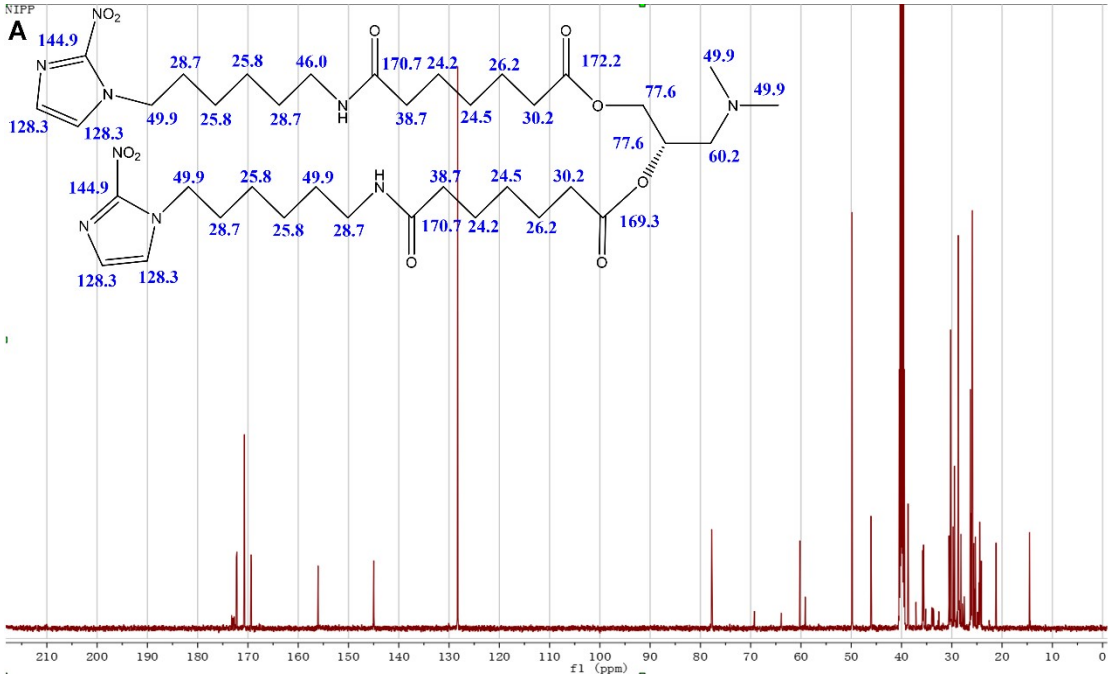

Figure S5. 13C NMR spectrum for NIPP in deuterated DMSO (DMSO-d6). The 13C-NMR spectrum of synthesized lipid NIPP was consistent with the proposed structure. The characteristic carbon chemical shift of -O-CO- were respectively 172.2 ppm and 169.3ppm. And the characteristic carbon chemical shift of -NH-CO- was 170.7 ppm. The carbon chemical shift of -CH=CH- on the imidazole ring was 128.3 ppm. And the carbon chemical shift of -C-NO_2 on the imidazole ring was 144.9 ppm. In addition, the carbon chemical shift of 156.1 ppm was the N, N-Dimethylformamide solvent peak of -CHO.

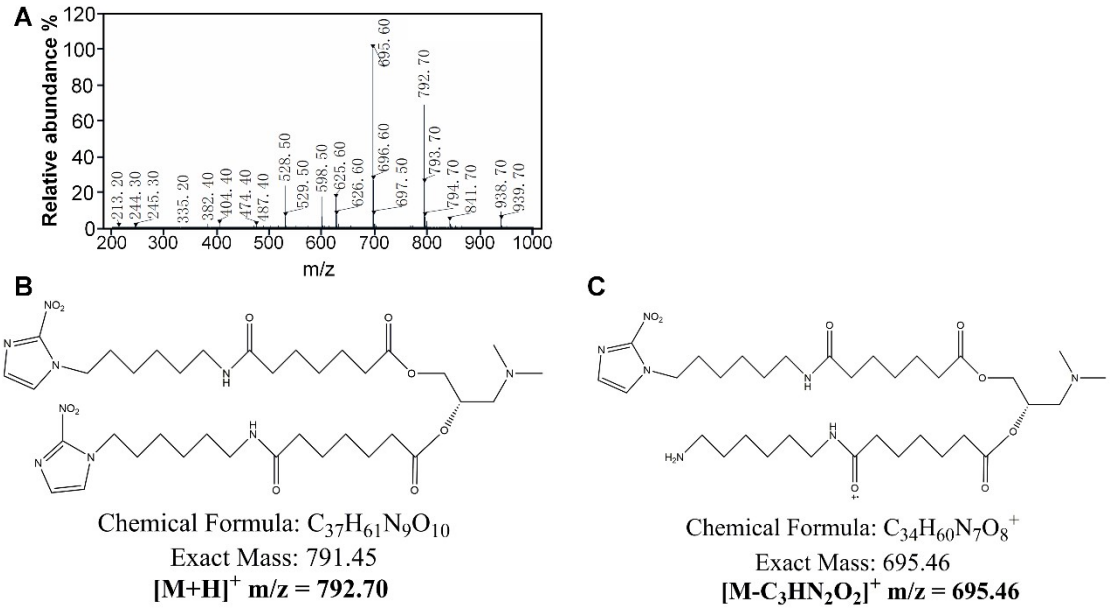

Figure S6. ESI-MS for NIPP. (A) Positive ion mass spectrum of NIPP at a mass-to-charge ratio (m/z) ranging from 200 Da to 1000 Da. (B) $[M + H]^+$ peak. (C) Possible structure of the m/z 695.46 fragment major ion peak.

Table S1. The hydrated particle size, zeta potential, drug loading and encapsulation efficiency of each nanoparticle.

nanoparticles	hydrodynamic diameter /nm	Polydispersity index	Zeta potential/mV	DL/%	EE/%
DOTAP	105.44±1.93	0.221±0.015	5.4±0.5	/	/
NIPP	132.66±4.61	0.250±0.011	-1.7±0.2	/	/
DOTAP/ER	161.25±3.40	0.144±0.015	2.2±0.4	11.55	51.49
NIPP/ER	154.75±3.20	0.242±0.008	-4.1±1.0	10.44	46.69
DOTAP/ER@HL-D	209.75±4.03	0.242±0.006	0.2±0.2	8.94	41.57
NIPP/ER@HL-D	210.25±5.25	0.232±0.021	-10.2±0.2	6.56	31.48

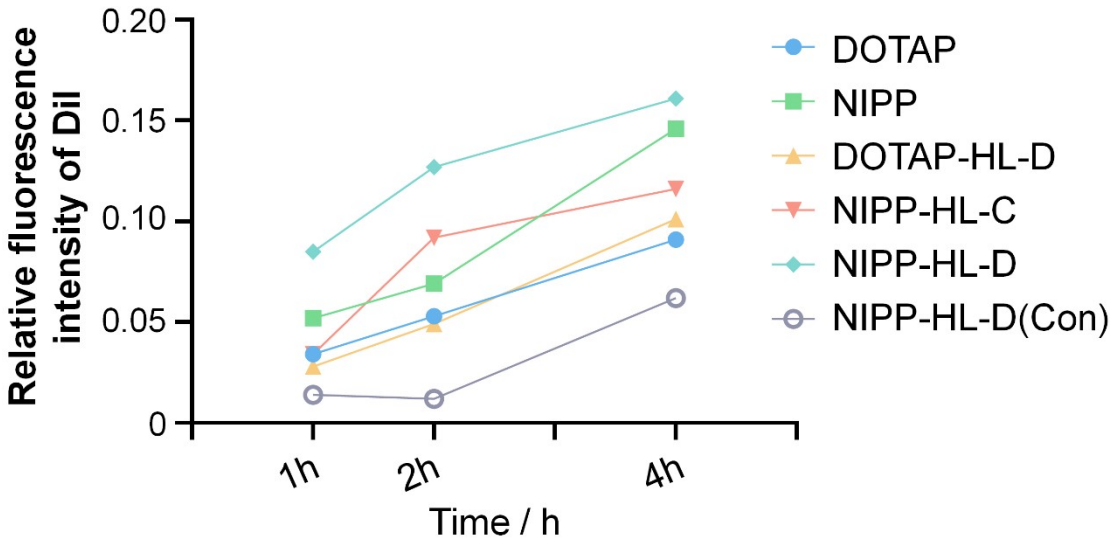

Figure.S7. The DiI relative fluorescence intensity of images in Figure.3A.

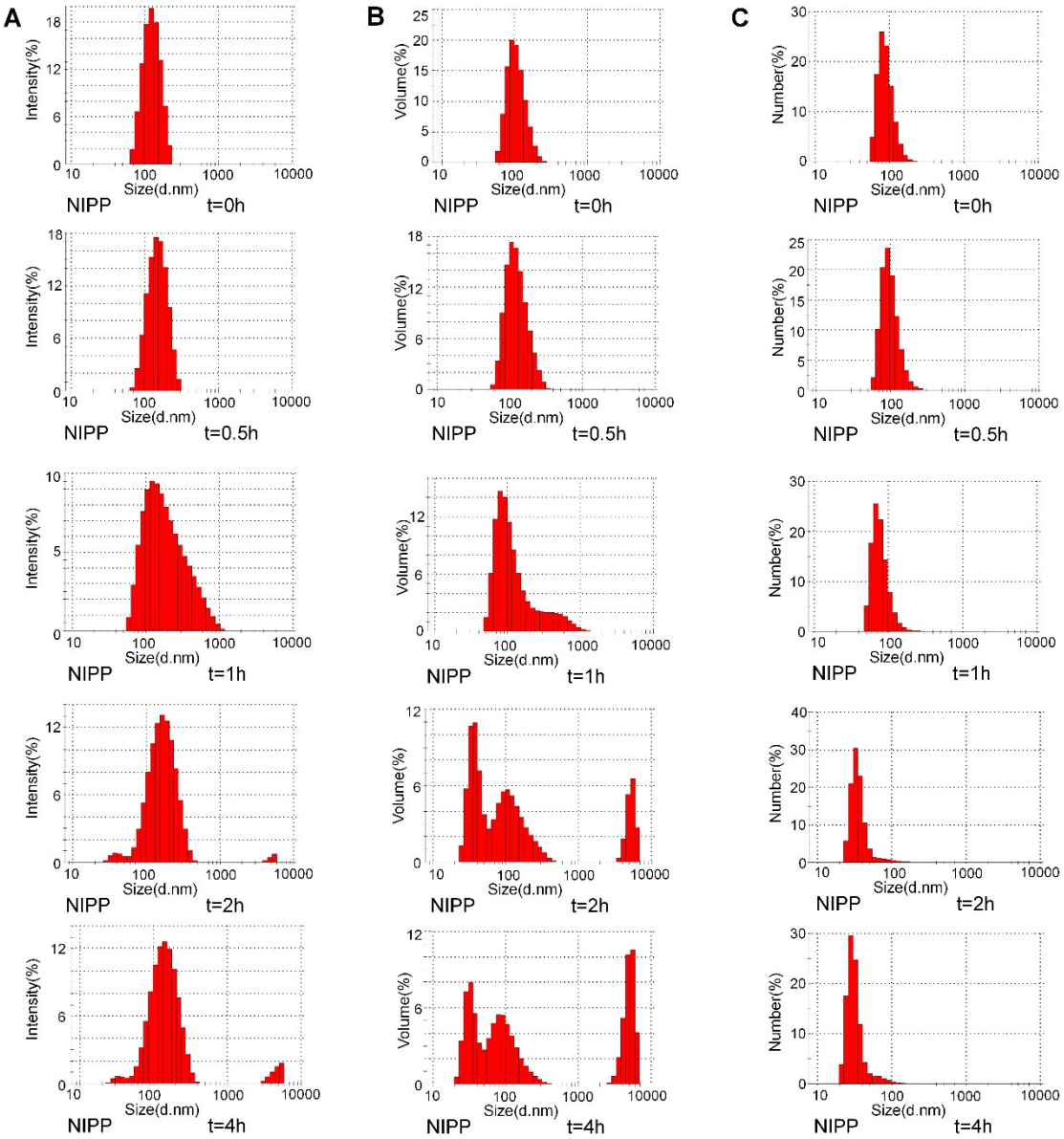

Figure.S8. The changes of size distributions of NIPP/ER liposomes at different time points under a simulated hypoxic microenvironment. (A) The intensity-weighted particle size distribution. (B) The volume-weighted particle size distribution. (C) The number-weighted particle size distribution.

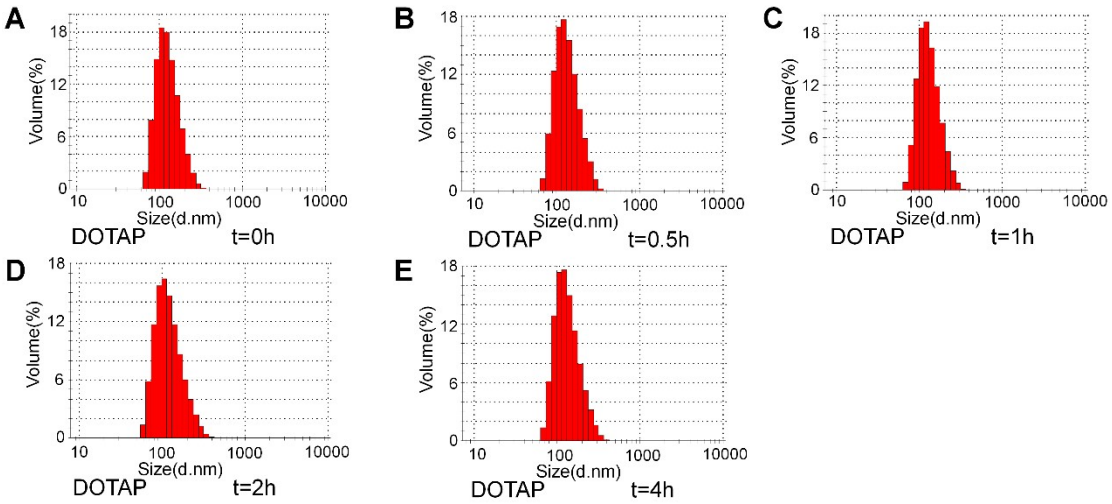

Figure S9. The changes of the volume-weighted particle size distribution of the DOTAP liposomes at different time points under a simulated hypoxic microenvironment.

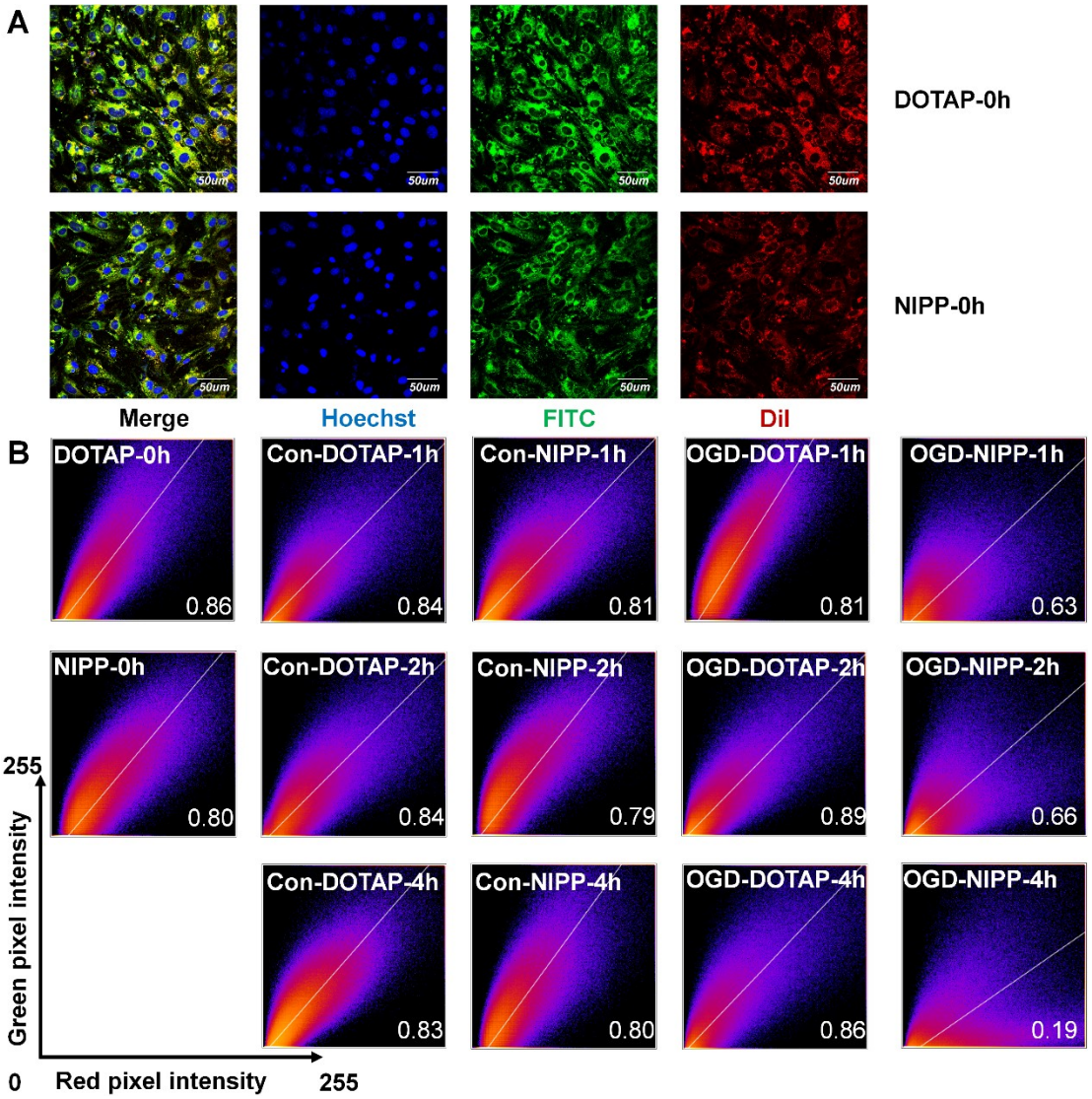

Figure S10. Hypoxia-sensitive properties of the NIPP liposomes. (A) After 4 h cellular uptake under normal culture conditions, the intracellular release of liposomes DOTAP was like liposomes NIPP, which was beneficial to the evaluation of the hypoxia-sensitive properties of the NIPP liposomes under OGD condition. (B) The intracellular hypoxia-sensitive releases in Fig.3D was characterized by the co-localized pixels of scatter plots and their Pearson's correlation coefficients (PCCs) between red fluorescence (DiI) and green fluorescence (FITC). PCCs were marked at the lower right corner of the scatter plots.

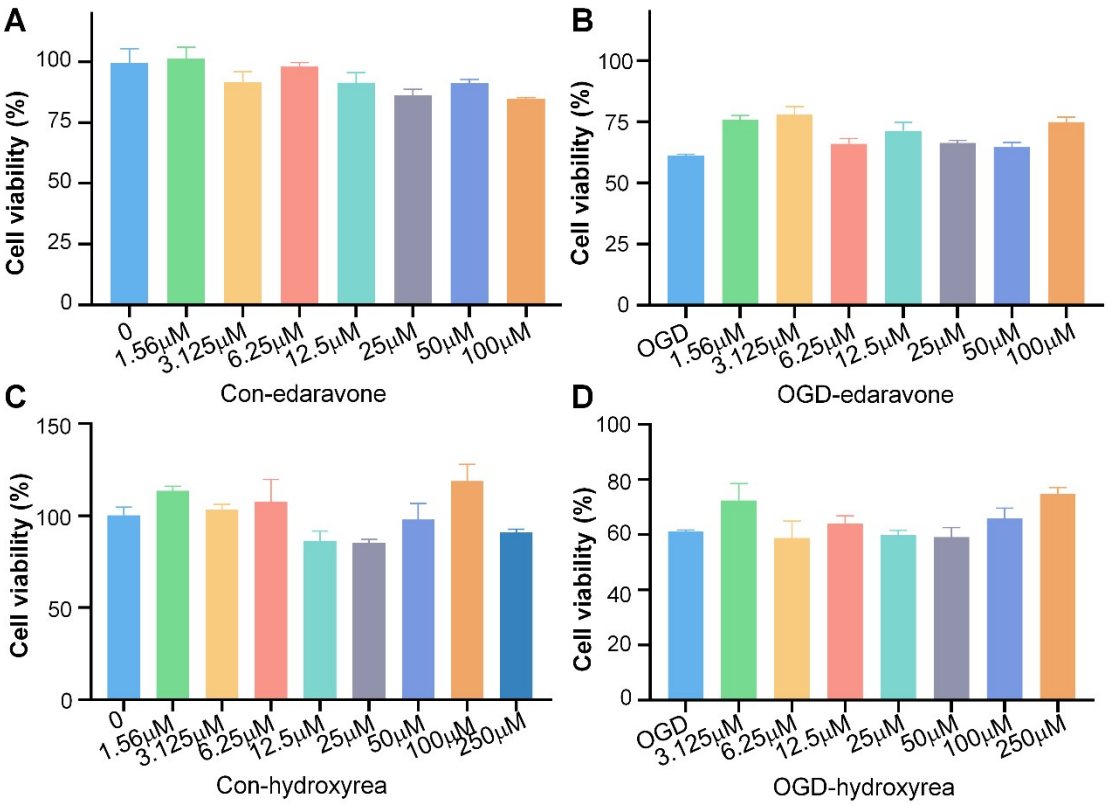

Figure S11. The optimal dose of edaravone and hydroxyrea was determined by MTT assay in bEnd.3 cells under OGD conditions for 12 h. (A) Cell survival rate of edaravone at 0~100 μM under normal conditions for 12 h. (B) Cell survival rate of edaravone at 0~100 μM under OGD conditions for 12 h. (C) Cell survival rate of hydroxyrea at 0~250 μM under normal conditions for 12 h. (D) Cell survival rate of hydroxyrea at 0~250 μM under OGD conditions for 12 h.

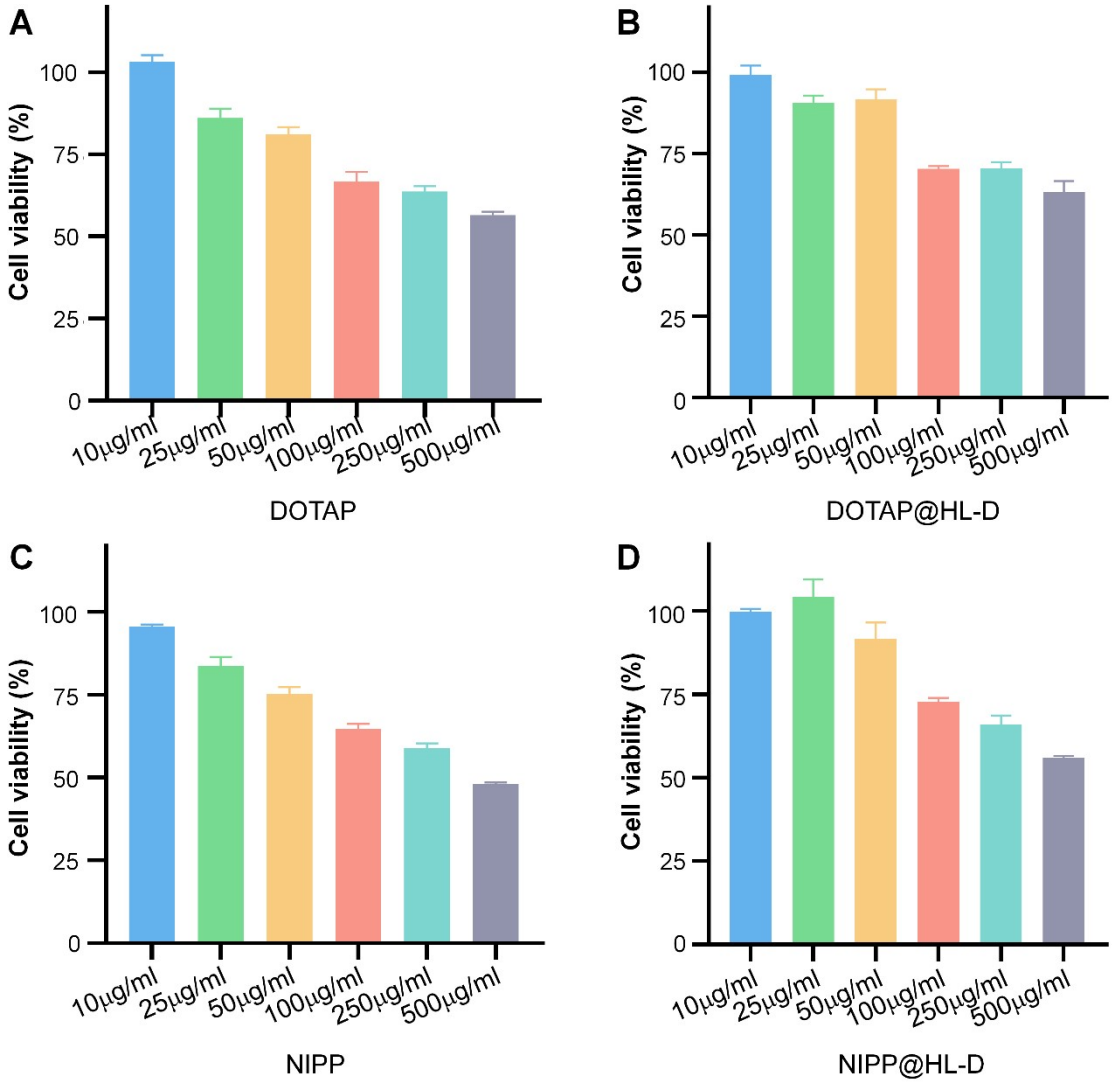

Figure S12. The toxicity evaluation of blank carriers. (A) Cell survival rate of liposomes DOTAP at 10 μg/mL~500 μg/mL under OGD conditions for 12 h. (B) Cell survival rate of liposomes DOTAP@HL-D at 10 μg/mL~500 μg/mL under OGD conditions for 12 h. (C))Cell survival rate of liposomes NIPP at 10 μg/mL~500 μg/mL under OGD conditions for 12 h. (D) Cell survival rate of liposomes NIPP@HL-D at 10 μg/mL~500 μg/mL under OGD conditions for 12 h. The cell viability was calculated as the ratio of the absorbance of each group to OGD group.

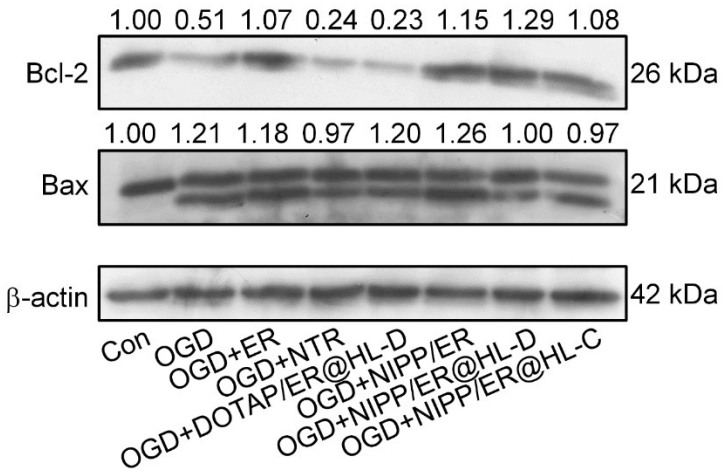

Figure S13. The Western Blot analyses of anti-apoptosis protein Bcl-2 and pro-apoptosis protein Bax in bEnd.3 cells after different treatments under 12h OGD or normal conditions.

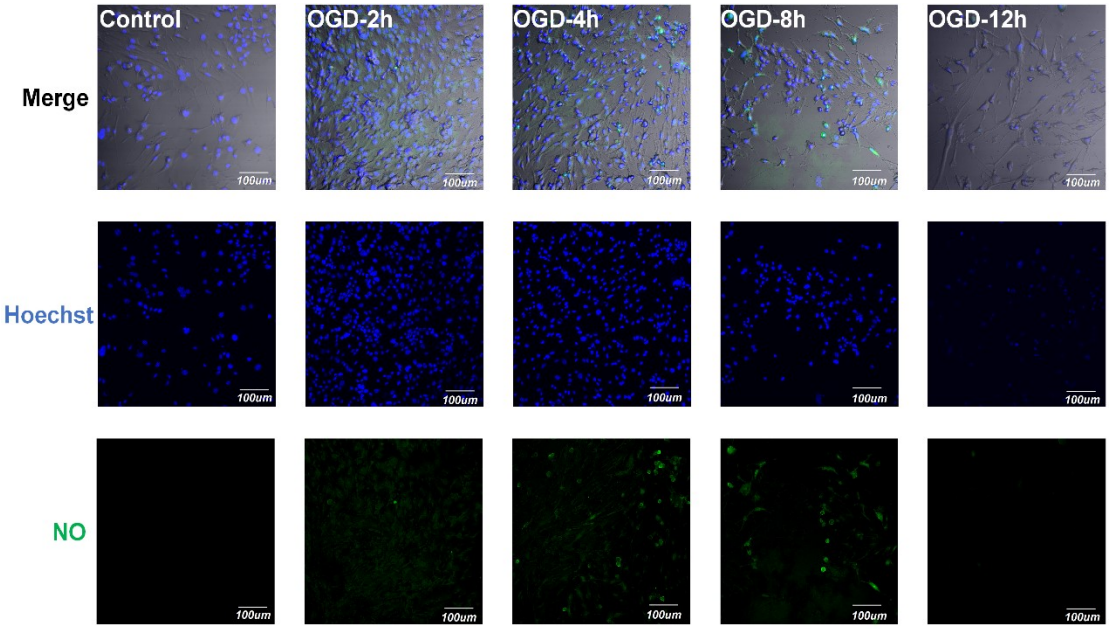

Figure S14. Changs of NO production with the duration of OGD (0h, 2h, 4h, 8h, 12h) in bEnd.3 cells.

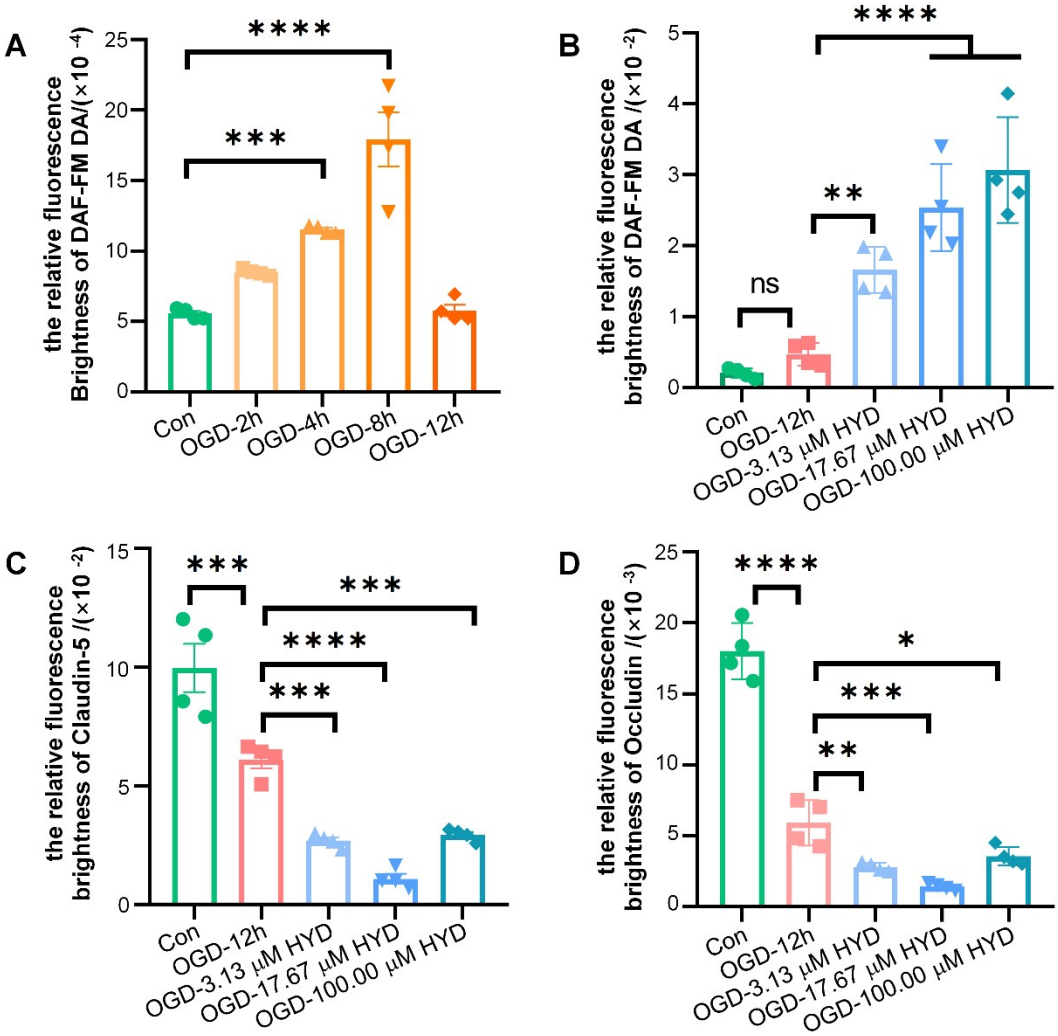

Figure S15. Quantitative results of immunofluorescence. (A) The immunofluorescence quantitative results of the changs of NO production with the duration of OGD (0h, 2h, 4h, 8h, 12h) in bEnd.3 cells in Figure.S8. (B) The immunofluorescence quantitative results of NO production in bEnd.3 cells treated with different concentrations of HYD (0, 3.13μM, 17.67 μM and 100μM) under OGD condition in Fig.4C. (C) The immunofluorescence quantitative results of the changs of tight junction protein claudin-5 in bEnd.3 cells treated with different concentrations of HYD under OGD condition in Fig.4C. (D) The immunofluorescence quantitative results of the changs of tight junction protein occludin in bEnd.3 cells treated with different concentrations of HYD under OGD condition in Fig.4C.

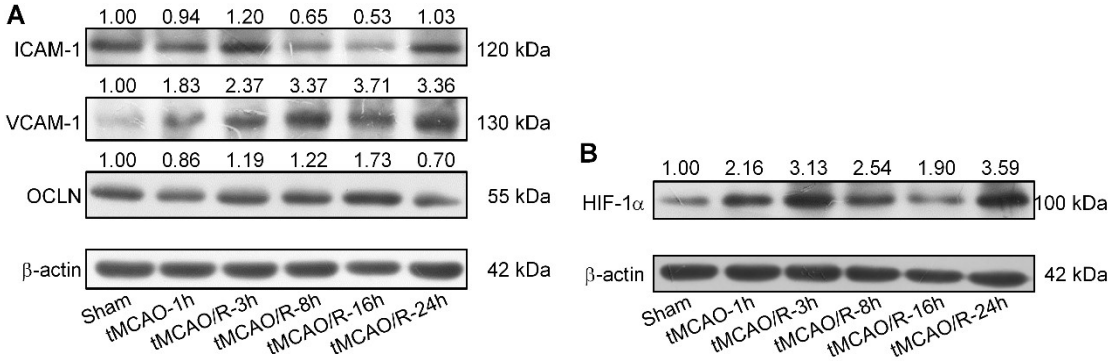

Figure S16. The protein expressions of ICAM-1, VCAM-1, occludin (OCLN) and HIF-1α were measured by WB analyses in lesioned tissue of cerebral ischemic rats subjected to different ischemic time.

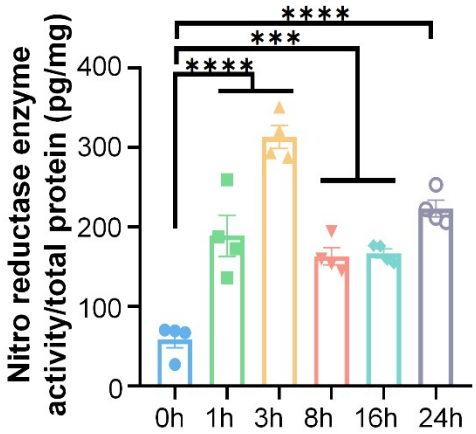

Figure S17. The nitro reductase enzyme activity was detected by ELISA in lesioned tissue of brain ischemic rats subjected to different ischemic times.

Electrophoretic gels and blots.

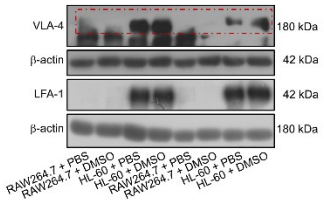

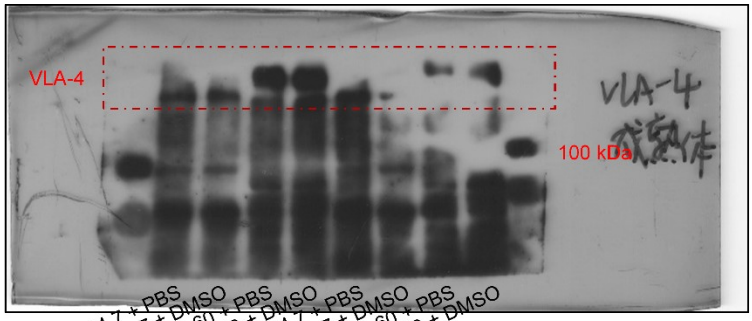

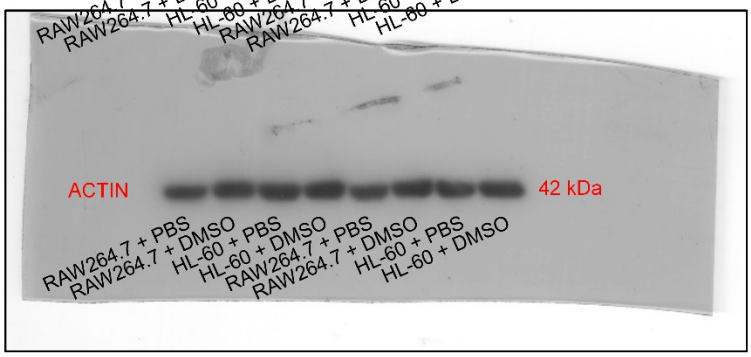

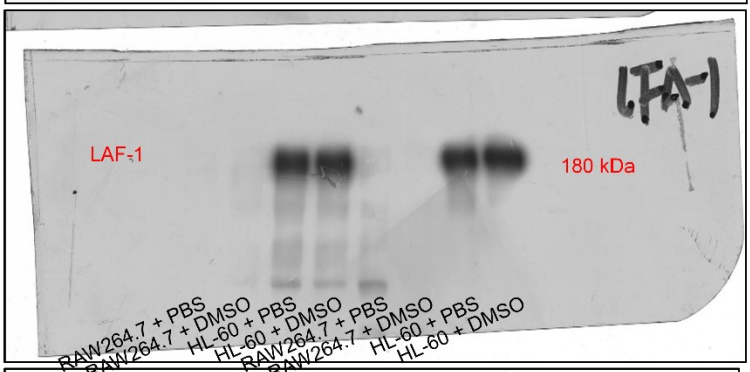

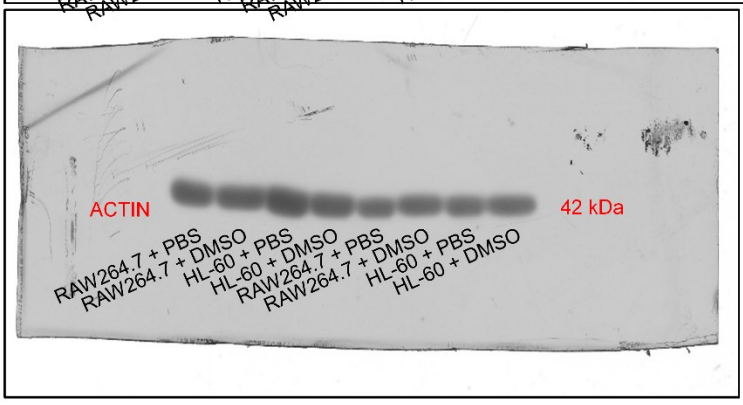

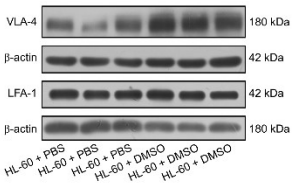
VLA-4
180 kDa
β-actin
42 kDa
LFA-1
42 kDa
β-actin
180 kDa
HL-60 + PBS
HL-60 + PBS
HL-60 + PBS
HL-60 + DMSO
HL-60 + DMSO
HL-60 + DMSO

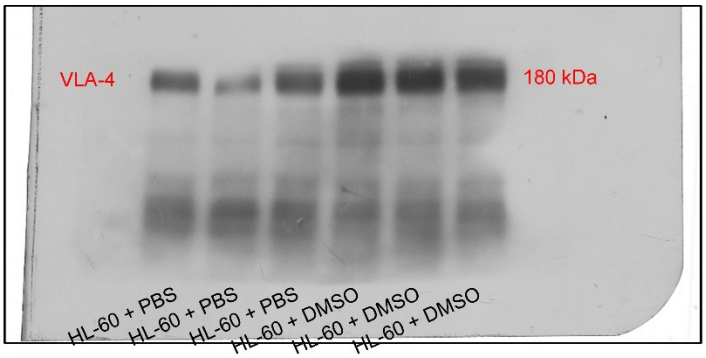
VLA-4
180 kDa
HL-60 + PBS
HL-60 + PBS
HL-60 + PBS
HL-60 + DMSO
HL-60 + DMSO
HL-60 + DMSO

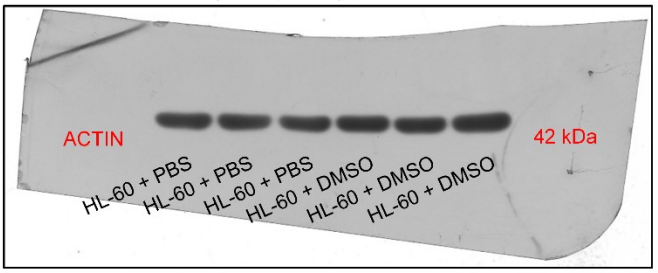
ACTIN
42 kDa
HL-60 + PBS
HL-60 + PBS
HL-60 + PBS
HL-60 + DMSO
HL-60 + DMSO
HL-60 + DMSO

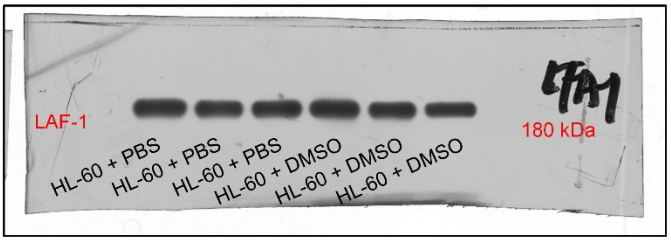
LAF-1
180 kDa
HL-60 + PBS
HL-60 + PBS
HL-60 + PBS
HL-60 + DMSO
HL-60 + DMSO
HL-60 + DMSO

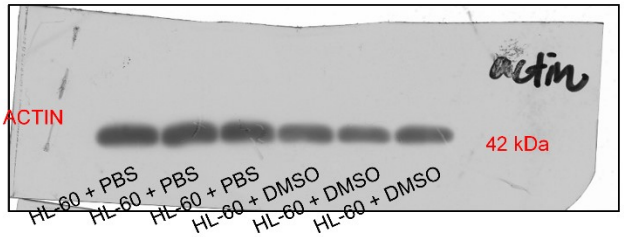
ACTIN
42 kDa
HL-60 + PBS
HL-60 + PBS
HL-60 + PBS
HL-60 + DMSO
HL-60 + DMSO
HL-60 + DMSO

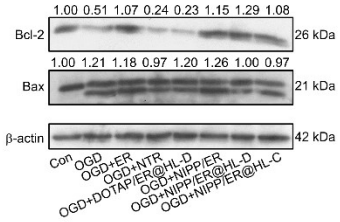
1.00 0.51 1.07 0.24 0.23 1.15 1.29 1.08
Bcl-2
26 kDa
1.00 1.21 1.18 0.97 1.20 1.26 1.00 0.97
Bax
21 kDa
β-actin
42 kDa
Con
OGD
OGD+ER
OGD+NTR
OGD+DOTAP/ER@HL-D
OGD+NIPP/ER
OGD+NIPP/ER@HL-D
OGD+NIPP/ER@HL-C

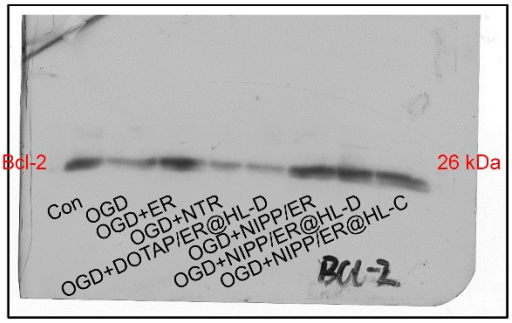
Bcl-2
26 kDa
Con
OGD
OGD+ER
OGD+NTR
OGD+DOTAP/ER@HL-D
OGD+NIPP/ER
OGD+NIPP/ER@HL-D
OGD+NIPP/ER@HL-C

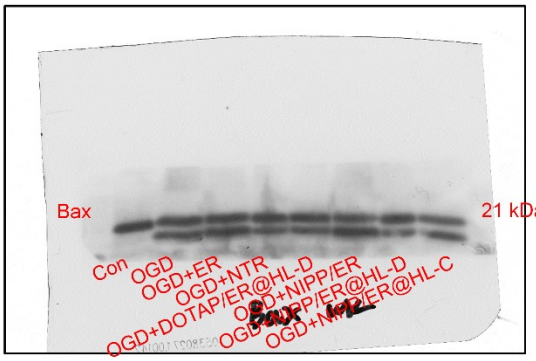
Bax
21 kDa
Con
OGD
OGD+ER
OGD+NTR
OGD+DOTAP/ER@HL-D
OGD+NIPP/ER
OGD+NIPP/ER@HL-D
OGD+NIPP/ER@HL-C

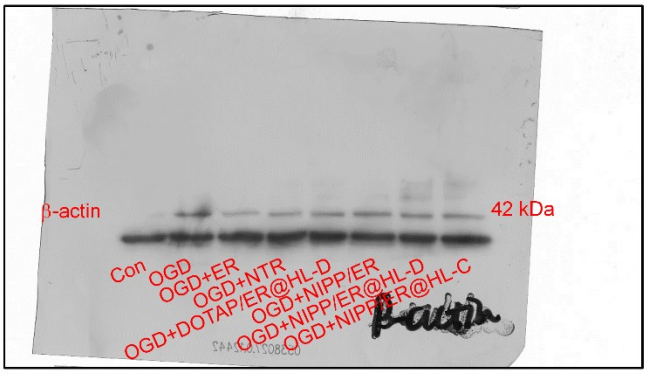
β-actin
42 kDa
Con
OGD
OGD+ER
OGD+NTR
OGD+DOTAP/ER@HL-D
OGD+NIPP/ER
OGD+NIPP/ER@HL-D
OGD+NIPP/ER@HL-C

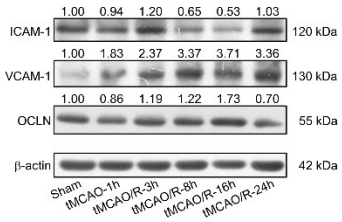
1.00 0.94 1.20 0.65 0.53 1.03
ICAM-1
120 kDa
1.00 1.83 2.37 3.37 3.71 3.36
VCAM-1
130 kDa
1.00 0.86 1.19 1.22 1.73 0.70
OCLN
55 kDa
β-actin
42 kDa
Sham
tMCAO-1h
tMCAO/R-3h
tMCAO/R-8h
tMCAO/R-16h
tMCAO/R-24h

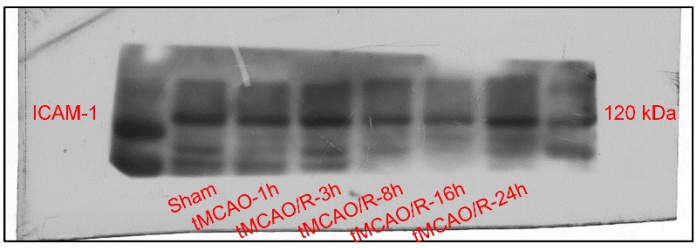
ICAM-1
120 kDa
Sham
tMCAO-1h
tMCAO/R-3h
tMCAO/R-8h
tMCAO/R-16h
tMCAO/R-24h

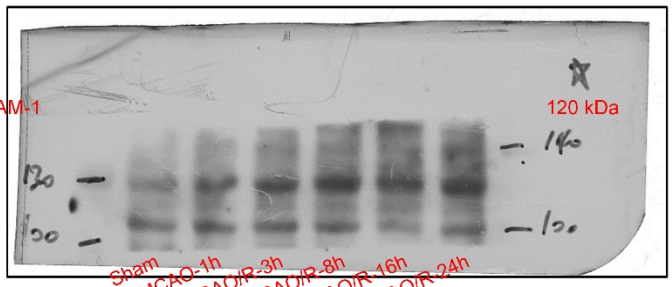
VCAM-1
120 kDa
Sham
tMCAO-1h
tMCAO/R-3h
tMCAO/R-8h
tMCAO/R-16h
tMCAO/R-24h

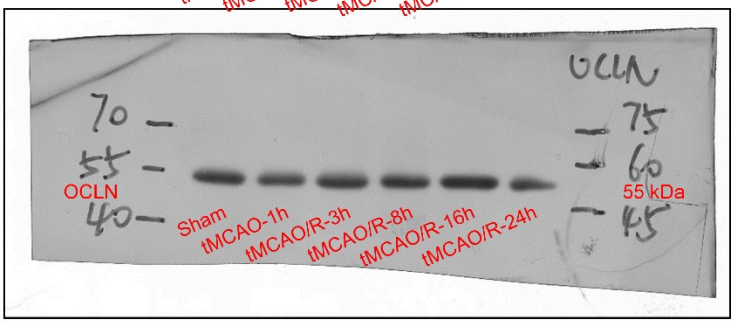
OCLN
55 kDa
Sham
tMCAO-1h
tMCAO/R-3h
tMCAO/R-8h
tMCAO/R-16h
tMCAO/R-24h

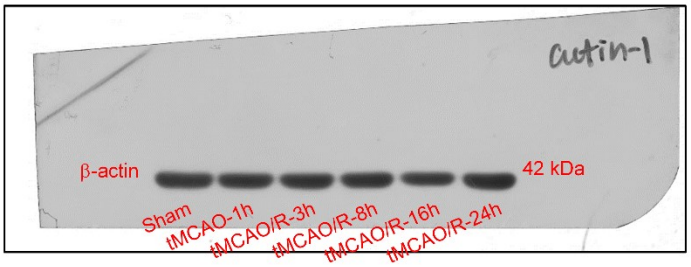
β-actin
42 kDa
Sham
tMCAO-1h
tMCAO/R-3h
tMCAO/R-8h
tMCAO/R-16h
tMCAO/R-24h

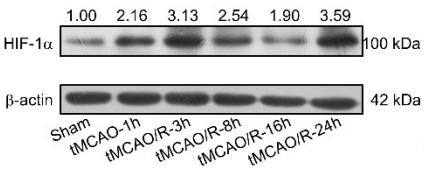
1.00 2.16 3.13 2.54 1.90 3.59
HIF-1α
100 kDa
β-actin
42 kDa
Sham
tMCAO-1h
tMCAO/R-3h
tMCAO/R-8h
tMCAO/R-16h
tMCAO/R-24h

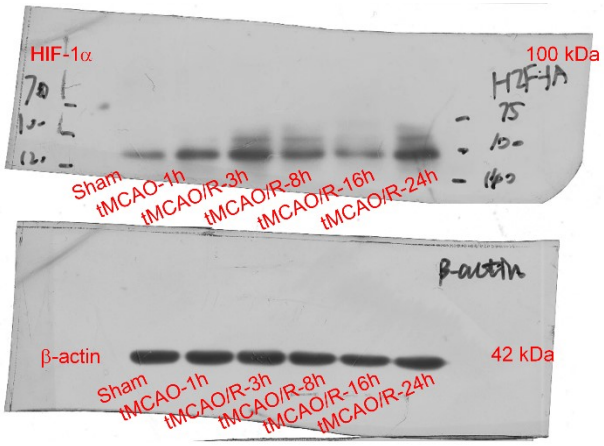
HIF-1α
100 kDa
β-actin
42 kDa
Sham
tMCAO-1h
tMCAO/R-3h
tMCAO/R-8h
tMCAO/R-16h
tMCAO/R-24h

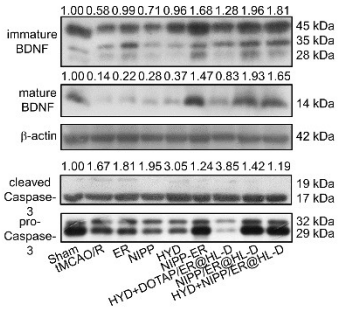
1.00 0.58 0.99 0.71 0.96 1.68 1.28 1.96 1.81
immature BDNF
45 kDa
35 kDa
28 kDa
1.00 0.14 0.22 0.28 0.37 1.47 0.83 1.93 1.65
mature BDNF
14 kDa
β-actin
42 kDa
1.00 1.67 1.81 1.95 3.05 1.24 3.85 1.42 1.19
cleaved Caspase-3
19 kDa
17 kDa
pro-Caspase-3
32 kDa
29 kDa
Sham
tMCAO/R
ER
NIPP
HYD
NIPP-ER
HYD+DOTAP/ER@HL-D
NIPP/ER@HL-D
HYD+NIPP/ER@HL-D

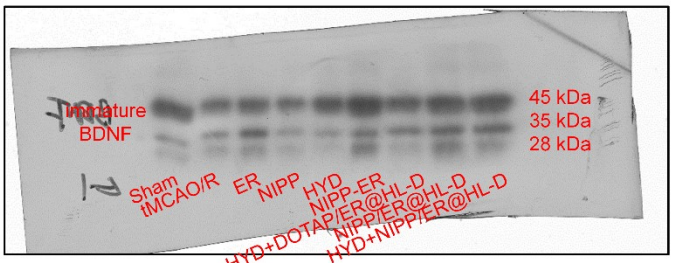
immature BDNF
45 kDa
35 kDa
28 kDa
Sham
tMCAO/R
ER
NIPP
HYD
NIPP-ER
HYD+DOTAP/ER@HL-D
NIPP/ER@HL-D
HYD+NIPP/ER@HL-D

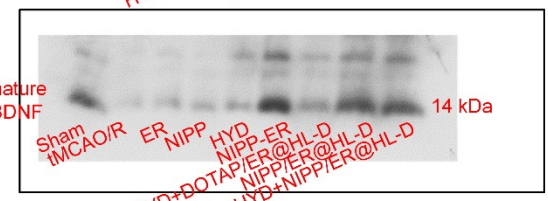
mature BDNF
14 kDa
Sham
tMCAO/R
ER
NIPP
HYD
NIPP-ER
HYD+DOTAP/ER@HL-D
NIPP/ER@HL-D
HYD+NIPP/ER@HL-D

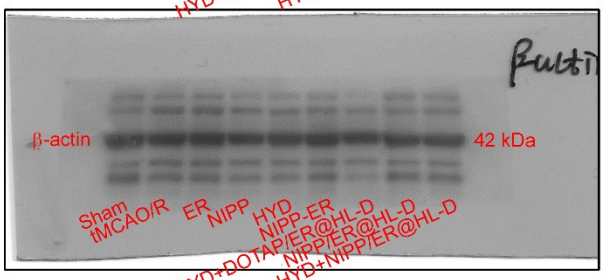
β-actin
42 kDa
Sham
tMCAO/R
ER
NIPP
HYD
NIPP-ER
HYD+DOTAP/ER@HL-D
NIPP/ER@HL-D
HYD+NIPP/ER@HL-D

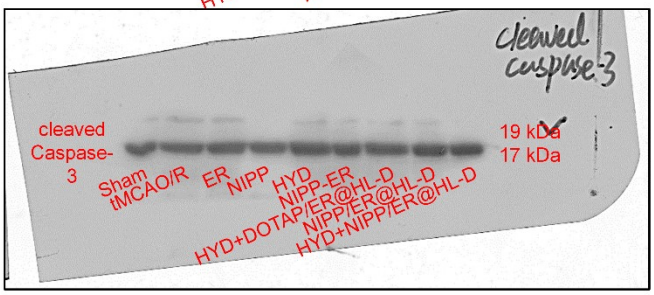
cleaved Caspase-3
19 kDa
17 kDa
Sham
tMCAO/R
ER
NIPP
HYD
NIPP-ER
HYD+DOTAP/ER@HL-D
NIPP/ER@HL-D
HYD+NIPP/ER@HL-D

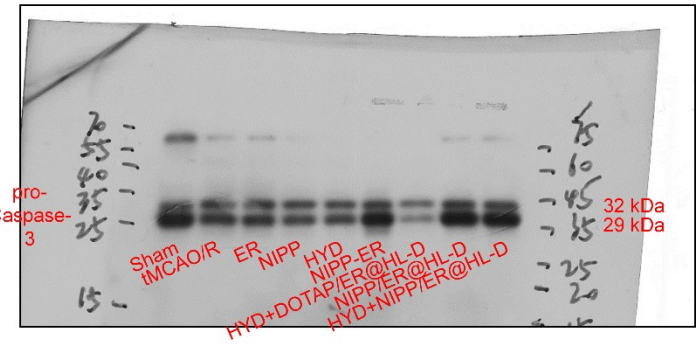
pro-Caspase-3
32 kDa
29 kDa
Sham
tMCAO/R
ER
NIPP
HYD
NIPP-ER
HYD+DOTAP/ER@HL-D
NIPP/ER@HL-D
HYD+NIPP/ER@HL-D

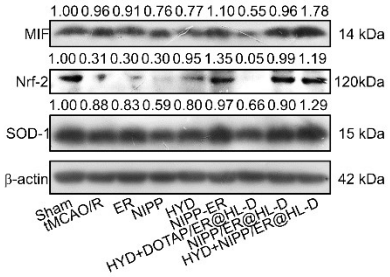
1.00 0.96 0.91 0.76 0.77 1.10 0.55 0.96 1.78
MIF
14 kDa
1.00 0.31 0.30 0.30 0.95 1.35 0.05 0.99 1.19
Nrf-2
120kDa
1.00 0.88 0.83 0.59 0.80 0.97 0.66 0.90 1.29
SOD-1
15 kDa
β-actin
42 kDa
Sham
tMCAO/R
ER
NIPP
HYD
NIPP-ER
HYD+DOTAP/ER@HL-D
NIPP/ER@HL-D
HYD+NIPP/ER@HL-D

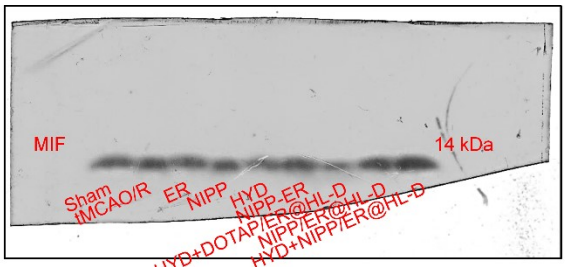
MIF
14 kDa
Sham
tMCAO/R
ER
NIPP
HYD
NIPP-ER
HYD+DOTAP/ER@HL-D
NIPP/ER@HL-D
HYD+NIPP/ER@HL-D

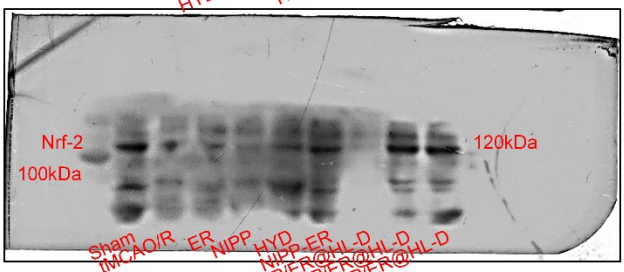
Nrf-2
100kDa
120kDa
Sham
tMCAO/R
ER
NIPP
HYD
NIPP-ER
HYD+DOTAP/ER@HL-D
NIPP/ER@HL-D
HYD+NIPP/ER@HL-D

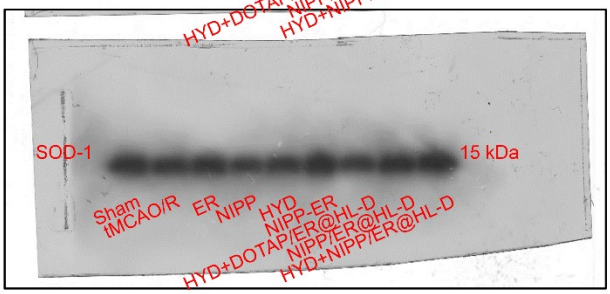
SOD-1
15 kDa
Sham
tMCAO/R
ER
NIPP
HYD
NIPP-ER
HYD+DOTAP/ER@HL-D
NIPP/ER@HL-D
HYD+NIPP/ER@HL-D

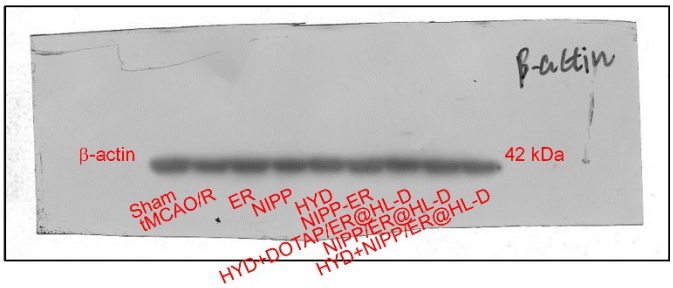
β-actin
β-actin
42 kDa
Sham
tMCAO/R
ER
NIPP
HYD
NIPP-ER
HYD+DOTAP/ER@HL-D
NIPP/ER@HL-D
HYD+NIPP/ER@HL-D